

1 **Enrichment of calcium in sea spray aerosol: Insights from bulk measurements**  
2 **and individual particle analysis during the R/V *Xuelong* cruise in the**  
3 **summertime Ross Sea, Antarctica**

4 Bojiang Su <sup>a,b</sup>, Xinhui Bi <sup>a,c</sup>, Zhou Zhang <sup>b,d</sup>, Yue Liang <sup>e</sup>, Congbo Song <sup>f</sup>, Tao Wang <sup>a,b</sup>, Yaohao  
5 Hu <sup>a,b</sup>, Lei Li <sup>g,\*</sup>, Zhen Zhou <sup>g</sup>, Jinpei Yan <sup>h</sup>, Xinming Wang <sup>a,c</sup>, Guohua Zhang <sup>a,c,\*</sup>

6 <sup>a</sup> State Key Laboratory of Organic Geochemistry and Guangdong Provincial Key Laboratory of  
7 Environmental Protection and Resources Utilization, Guangzhou Institute of Geochemistry,  
8 Chinese Academy of Sciences, Guangzhou 510640, China

9 <sup>b</sup> University of Chinese Academy of Sciences, Beijing 100049, China

10 <sup>c</sup> Guangdong-Hong Kong-Macao Joint Laboratory for Environmental Pollution and Control,  
11 Guangzhou 510640, China

12 <sup>d</sup> State Key Laboratory of Isotope Geochemistry, Guangzhou Institute of Geochemistry, Chinese  
13 Academy of Sciences, Guangzhou 510640, China

14 <sup>e</sup> Department of Civil and Environmental Engineering, Faculty of Science and Technology,  
15 University of Macau, Taipa, Macau, China

16 <sup>f</sup> National Centre for Atmospheric Science (NCAS), University of Manchester, Manchester M13  
17 9PL, UK

18 <sup>g</sup> Institute of Mass Spectrometry and Atmospheric Environment, Jinan University, Guangzhou  
19 510632, China

20 <sup>h</sup> Key Laboratory of Global Change and Marine Atmospheric Chemistry, Third Institute of  
21 Oceanography, Ministry of Natural Resources, Xiamen 361005, China

22 \*Corresponding author: [zhanggh@gig.ac.cn](mailto:zhanggh@gig.ac.cn); [lileishdx@163.com](mailto:lileishdx@163.com)

23 **Abstract:** Although calcium is known to be enriched in sea spray aerosols (SSAs), the factors that  
24 affect its enrichment remain ambiguous. In this study, we examine how environmental factors  
25 affect the distribution of water-soluble calcium ( $\text{Ca}^{2+}$ ) distribution in SSAs. We obtained our  
26 dataset from observations taken during a research cruise on the R/V *Xuelong* cruise in the Ross  
27 Sea, Antarctica, from December 2017 to February 2018. Our observations showed that the  
28 enrichment of  $\text{Ca}^{2+}$  in aerosol samples was enhanced under specific conditions, including lower  
29 temperatures ( $< -3.5$  °C), lower wind speeds ( $< 7$  m s<sup>-1</sup>), and the presence of sea ice. Our analysis  
30 of individual particle mass spectra revealed that a significant portion of calcium in SSAs was  
31 likely bound with organic matter (in the form of a single-particle type, OC-Ca). Our findings  
32 suggest that current estimations of  $\text{Ca}^{2+}$  enrichment based solely on water-soluble  $\text{Ca}^{2+}$  may be  
33 inaccurate. Our study is the first to observe a single-particle type dominated by calcium in the  
34 Antarctic atmosphere. Our findings suggest that future Antarctic atmospheric modeling should  
35 take into account the environmental behavior of individual OC-Ca. With the ongoing global  
36 warming and retreat of sea ice, it is essential to understand the mechanisms of calcium enrichment  
37 and the mixing state of individual particles to better comprehend the interactions between aerosols,  
38 clouds, and climate during the Antarctic summer.

39 **Key points:**

- 40 ●  $\text{Ca}^{2+}$  enrichment in sea spray aerosols (SSAs) was observed at lower ambient temperatures,  
41 lower wind speeds, and in the presence of sea ice.
- 42 ● Individual particle analysis revealed a significant portion of internally mixed organics with  
43 calcium particles in the Antarctic summer atmosphere.
- 44 ● Current water-soluble estimation of  $\text{Ca}^{2+}$  enrichment in SSAs may be inaccurate without  
45 considering organically complexed calcium.

46 **Keywords:**

47 Sea spray aerosol; Calcium enrichment; Individual particle analysis; Environmental factors;  
48 Internally mixed organics with calcium particles; Antarctic summer atmosphere.  
49

## 50 **1 Introduction**

51 Sea spray aerosols (SSAs) govern radiative forcing by directly scattering and absorbing solar  
52 radiation over the remote ocean (Murphy et al., 1998), and they affect the microphysical properties  
53 of marine clouds by serving as cloud condensation nuclei (CCN) and ice nuclei (IN) (Wilson et al.,  
54 2015; Brooks and Thornton, 2018; Willis et al., 2018). Calcium is one of the components of SSA,  
55 which can present as inorganic calcium (e.g.,  $\text{CaCl}_2$  and  $\text{CaSO}_4$ ) (Chi et al., 2015) as well as  
56 organic calcium (i.e.,  $\text{Ca}^{2+}$  can readily induce the gelation of organic matter, presenting as the most  
57 efficient gelling agent) (Carter-Fenk et al., 2021). Calcium enrichment and chemical signature can  
58 affect some physicochemical properties of SSAs such as alkalinity and hygroscopicity (Salter et  
59 al., 2016; Mukherjee et al., 2020), which is critical for understanding aerosol-cloud interactions  
60 over the remote marine boundary layer (Keene et al., 2007; Leck and Svensson, 2015; Bertram et  
61 al., 2018).

62 Several studies have demonstrated significant enrichment of calcium ( $\text{Ca}^{2+}$ ) in SSAs  
63 compared to bulk seawater, as briefly summarized in **Table S1** and documented by Keene et al.  
64 (2007), Hara et al. (2012), Cochran et al. (2016), Salter et al. (2016), Cravigan et al. (2020), and  
65 Mukherjee et al. (2020). For example, Hara et al. (2012) found that the  $\text{Ca}^{2+}$  enrichment of aerosol  
66 samples was sensitive to sea salt fractionation during the cold winter-spring season over the  
67 Antarctic coast. Leck and Svensson (2015) suggested that  $\text{Ca}^{2+}$  enrichment in SSAs is attributed to  
68 bubble bursts on sea ice leads over the Arctic area. Similarly, low wind-driven bubble bursts were  
69 regarded as a major reason for the  $\text{Ca}^{2+}$  enrichment in SSAs during an Arctic cruise (Mukherjee et  
70 al., 2020). These results shed light on the  $\text{Ca}^{2+}$  enrichment process; however, our understanding of  
71 how environmental factors synergistically affect such enrichment processes remains unclear.

72 To date, a unified consensus on the chemical form of calcium to explain calcium enrichment  
73 in SSAs has not been reached. Two hypotheses have been proposed: (i) Calcium enrichment is  
74 dominated by inorganic calcium, such as  $\text{CaCO}_3$  and  $\text{CaCl}_2$ .  $\text{Ca}^{2+}$  is enriched close to the seawater  
75 surface in the form of ionic clusters (most probably with carbonate ions) (Salter et al., 2016).  
76 Another source of  $\text{CaCO}_3$  is directly from calcareous shell debris (Keene et al., 2007). Through  
77 bubble bursts, both  $\text{CaCO}_3$  and  $\text{CaCl}_2$  along with sea salt can be emitted into the atmosphere. In  
78 addition, the sea salt fractionation by precipitation of ikaite ( $\text{CaCO}_3 \cdot 6\text{H}_2\text{O}$ ) may contribute to  
79 calcium enrichment in aerosol during the freezing of sea ice (Hara et al., 2012). (ii) Calcium  
80 enrichment is attributed to organically complexed calcium.  $\text{Ca}^{2+}$  may bind with organic matter,  
81 which is relevant with marine microgels and/or coccolithophore phytoplankton scales, and can be  
82 emitted by bubble bursting (Oppo et al., 1999; Sievering, 2004; Leck and Svensson, 2015;  
83 Cochran et al., 2016; Kirpes et al., 2019; Mukherjee et al., 2020). The chemical form of calcium  
84 can determine its atmospheric role. Inorganic calcium may exhibit stronger aerosol alkalinity and  
85 hygroscopicity than organic calcium (Salter et al., 2016; Mukherjee et al., 2020). However, current  
86 estimations of calcium enrichment based solely on water-soluble  $\text{Ca}^{2+}$  may not precisely explain  
87 the calcium distribution in SSAs. This is because the amount of low water-soluble complexation  
88 of  $\text{Ca}^{2+}$  with organic matter (e.g., aged  $\text{Ca}^{2+}$ -assembled gel-like particles) (Orellana and Verdugo,  
89 2003; Leck and Bigg, 2010; Russell et al., 2010; Orellana et al., 2011; Leck and Svensson, 2015)  
90 and insoluble  $\text{Ca}^{2+}$  in the form of calcareous shell debris or the like may not be considered. Thus,  
91 an alternative method, such as discerning the mixing state based on single-particle analysis, may  
92 provide unique insights into the chemical form of calcium, and thus the mechanisms of calcium  
93 enrichment in SSAs.

94 As a part of the 34<sup>th</sup> Chinese Antarctic Research Expedition (CHINARE ANT34th), this  
95 study aimed to investigate the influencing factors and possible mechanisms of calcium enrichment  
96 in SSAs through R/V *Xuelong* cruise observation campaigns over the Ross Sea, Antarctica. An in-  
97 situ gas and aerosol composition monitoring system (IGAC) was employed to determine the  
98 extent of Ca<sup>2+</sup> enrichment in SSAs. Single-particle aerosol mass spectrometry (SPAMS) was  
99 utilized to measure the size and chemical signature (i.e., mixing state) of individual calcareous  
100 particles. We first investigated the impact of environmental factors such as ambient temperature,  
101 wind speed, sea ice fraction, chlorophyll-a concentration, and back trajectory coverage on Ca<sup>2+</sup>  
102 enrichment in SSAs. Then, the mechanisms of calcium enrichment in SSAs were inferred  
103 according to the mixing state of individual calcareous particles.

## 104 **2 Methodology**

### 105 **2.1 The R/V *Xuelong* cruise and observation regions**

106 Our study focused on the Ross Sea region of Antarctica (50 to 78° S, 160 to 185° E) (**Fig. 1**),  
107 where we conducted two separate observation campaigns aboard the R/V *Xuelong*. During the  
108 observations, this region was relatively isolated from the impact of long-range transport of  
109 anthropogenic aerosols and has experienced the sea ice retreat (Yan et al., 2020a).

110 The first observation campaign (Leg I) took place from December 2-20, 2017, during the sea  
111 ice period. The second campaign (Leg II) was conducted from January 13 to February 14, 2018,  
112 during the period without sea ice. The sampling design for Leg I and Leg II aimed to investigate  
113 how changing environmental factors affect the enrichment extent of calcium and the  
114 characteristics of individual particles.

## 115 2.2 Meteorological parameters and satellite data of air masses, sea ice, and chlorophyll-a

116 We measured various meteorological parameters, such as ambient temperature, relative  
117 humidity (RH), wind speed, and true wind direction using an automated meteorological station  
118 located on the top deck of the R/V *Xuelong* (Fig. S1 and Table S2).

119 To determine the type of air masses, we first overviewed the 72-hour back trajectory with  
120 daily resolution per each starting location by using the NOAA Hybrid Single-Particle Lagrangian  
121 Integrated Trajectories (HYSPLIT, version 4.9) model (Fig. S2). Additionally, we conducted a 96-  
122 hour back trajectory analysis with an hourly resolution, which covered the enhanced calcium  
123 enrichment events associated with sea ice fraction and chlorophyll-a concentration (discussed in  
124 section 3.1), using the TrajStat in Meteoinfo (version 3.5.8) (Wang et al., 2009; Wang, 2014).  
125 Meteorological data used for back trajectory analysis obtained from the Global Data Assimilation  
126 System (GDAS, <ftp://ftp.arl.noaa.gov/pub/archives>). Moreover, we obtained the monthly sea ice  
127 fraction from the Sea Ice Concentration Climate Data Record with a spatial resolution of 25 km  
128 (<https://www.ncei.noaa.gov/products/climate-data-records/sea-ice-concentration>) and the 8-day  
129 chlorophyll-a concentration from MODIS-aqua with a spatial resolution of 4 km  
130 (<https://modis.gsfc.nasa.gov>) (Fig. S3).

131 During the R/V *Xuelong* cruise observation campaigns, leg I was dominantly affected by the  
132 air masses from the sea ice-covered open water (92%, by trajectory coverage), and leg II was  
133 mainly affected by the air masses from continental Antarctica (58%) (Table S2). The average  
134 ambient temperature ( $-4.0 \pm 1.4$  °C vs.  $-3.1 \pm 2.2$  °C), wind speed ( $7.2 \pm 5.5$  m s<sup>-1</sup> vs.  $7.1 \pm 4.2$  m  
135 s<sup>-1</sup>), and chlorophyll-a concentration ( $0.51 \pm 0.29$  µg L<sup>-1</sup> vs.  $0.44 \pm 0.18$  µg L<sup>-1</sup>) varied slightly  
136 between the legs I and II (Table S2).

### 137 **2.3 Contamination control during observation campaigns**

138 During the research cruise, the major contamination source was identified as emissions from  
139 a chimney located at the stern of the vessel and about 25 m above the sea surface. To mitigate the  
140 potential impact of ship emissions on aerosol sampling, we have taken several measures. Firstly, a  
141 total suspended particulate (TSP) sampling inlet connecting to the monitoring instruments was  
142 fixed to a mast 20 m above the sea surface, located at the bow of the vessel. In addition, the  
143 sampling inlet was fixed on a ship pillar with a rain cover, which could minimize the potential  
144 influence of violent shaking of the ship and sea waves. Secondly, sampling was only conducted  
145 while the ship was sailing, to avoid the possible effect of ship emission on aerosol sampling under  
146 the low diffusion condition. Lastly, we did not observe the mass spectral characteristics associated  
147 with ship emission (e.g., particles simultaneously contain  $m/z$  51  $[V]^+$ , 67  $[VO]^+$ , and element  
148 carbon) during the observation campaigns (Liu et al., 2017; Passig et al., 2021). These measures  
149 ensured that the collected data were representative and reliable for subsequent analysis.

### 150 **2.4 Instrumentation**

151 An IGAC (Model S-611, Machine Shop, Fortelice International Co. Ltd.) and a SPAMS  
152 (Hexin Analytical Instrument Co., Ltd.) were synchronously employed to determine water-soluble  
153 ion mass concentrations of bulk aerosol and the size and chemical composition of individual  
154 particles in real-time with hourly resolution (**Figs. 2** and **S4**). In the aerosol sampling procedure, a  
155 TSP inlet with a  $PM_{10}$  cyclone (trap efficiency greater than 99% for particles  $> 0.3 \mu\text{m}$ ,  $D_{a50} = 10$   
156  $\pm 0.5 \mu\text{m}$ ) was used for IGAC sampling and a  $PM_{2.5}$  cyclone ( $D_{a50} = 2.5 \pm 0.2 \mu\text{m}$ ) to remove  
157 particles larger than  $2.5 \mu\text{m}$  for SPAMS. All instruments were connected using conductive silicon



158 tubing with an inner diameter of 1.0 cm.

#### 159 **2.4.1 Aerosol water-soluble ion constituents**

160 The details of the analytical method of IGAC have been described in previous studies (Young  
161 et al., 2016; Yan et al., 2019; Yan et al., 2020b). Briefly, the IGAC system consisted of three main  
162 units, including a Wet Annular Denuder (WAD), a Scrub and Impact Aerosol Collector (SIAC),  
163 and an ion chromatograph (IC, Dionex ICS-3000) (**Fig. 2**). Gases and aerosols were passed  
164 through WAD with a sampling flow of 16.7 L min<sup>-1</sup>. Two concentric Pyrex glass cylinders with a  
165 length of 50 cm and inner and outer diameters of 1.8 and 2.44 cm were assembled to WAD, in  
166 which the inner walls of the annulus were wetted with ultrapure water (18.2 MΩ cm<sup>-1</sup>). This part  
167 was responsible for the collection of acidic and basic gases by diffusion and absorption of a  
168 downward-flowing aqueous solution. The SIAC had a length of 23 cm and a diameter of 4.75 cm,  
169 which was positioned at an angle to facilitate the collection of enlarged particles. The collected  
170 particles were separated firstly, continually enlarged by vapor steam, and then accelerated through  
171 a conical-shaped impaction nozzle and collected on an impaction plate. Each aerosol sample was  
172 collected for 55 minutes and injected for 5 minutes. The injection loop size was 500 μL for both  
173 anions and cations, which were subsequently analyzed by IC. The collection efficiency of aerosol  
174 and gas samples before they entered IC was previously reported higher than 89% (for 0.056 μm  
175 particles, 89%; for 1 μm particles, 98%; for gas samples, > 90%) (Chang et al., 2007; Tian et al.,  
176 2017). The target ion concentrations were calibrated with a coefficient of determination (r<sup>2</sup>) above  
177 0.99 by using standard solutions (0.1-2000 μg L<sup>-1</sup>). The detection limits for Na, Cl, Ca, K, and Mg  
178 were 0.03, 0.03, 0.019, 0.011, and 0.042 μg L<sup>-1</sup> (aqueous solution), respectively. The systematic

179 error of the IC systems was generally less than 5%. The detection limits for Na<sup>+</sup>, Cl<sup>-</sup>, Ca<sup>2+</sup>, K<sup>+</sup>, and  
180 Mg<sup>2+</sup> were 0.03, 0.03, 0.019, 0.011, and 0.042 µg L<sup>-1</sup> (aqueous solution), respectively.

181 Throughout the observation campaigns, the mean Na<sup>+</sup> and Ca<sup>2+</sup> mass concentrations were  
182 364.64 ng m<sup>-3</sup> (ranging from 6.66 to 4580.10 ng m<sup>-3</sup>) and 21.20 ng m<sup>-3</sup> (ranging from 0.27 to  
183 334.40 ng m<sup>-3</sup>), respectively, which were 10 times higher than the detection limits. Analytical  
184 uncertainty of Ca<sup>2+</sup> enrichment based on water-soluble analysis was estimated at less than 11%  
185 **(Supporting Information, SI text S1).**

186 It should be clarified that the water-soluble ion mass concentration included the pure  
187 inorganic part (e.g., pure sea salt, NaCl) and mixed organic-inorganic part (e.g., gel-like particles)  
188 (Quinn et al., 2015). Numerous studies have reported that primary SSAs exhibited moderate  
189 hygroscopicity and water solubility due to a certain water-soluble organic fraction (~ 25%, by  
190 mass), such as carboxylates, lipopolysaccharides (LPSs), humic substances, and galactose (Oppo  
191 et al., 1999; Quinn et al., 2015; Schill et al., 2015; Cochran et al., 2017). For example, Oppo et al.  
192 (1999) indicated that humic substances were an important pool of water-soluble natural surfactants  
193 (40-60%) in marine surfactant organic matter. In addition, LPSs are preferentially transferred to  
194 submicron SSAs during bubble bursting and exhibit a certain solubility of 5 g L<sup>-1</sup> in pure water.  
195 (Facchini et al., 2008; Schill et al., 2015). Therefore, both organic and inorganic parts with a  
196 water-soluble nature could be retained, contributing to the water-soluble ion mass concentration  
197 (e.g., Ca<sup>2+</sup>).

#### 198 **2.4.2 Single-particle analysis**

199 A brief description of SPAMS has been provided elsewhere (Li et al., 2011). Briefly, the

200 aerosols were drawn into SPAMS by a PM<sub>2.5</sub> inlet after a silica gel dryer (**Fig. 2**). A collimated  
201 particle beam focused by an aerodynamic lens was then accelerated in an accelerating electric  
202 field and passed through two continuous laser beams (Nd: YAG laser, 532 nm). The obtained time  
203 of flight (TOF) and velocity of individual particles were used to calculate the vacuum  
204 aerodynamic diameter ( $D_{va}$ ) based on a calibration curve. Subsequently, particles with a specific  
205 velocity were desorbed and ionized by triggering a pulse laser (an Nd: YAG laser, 266 nm,  $0.6 \pm$   
206  $0.06$  mJ was used in this study). The ion fragments were recorded using a bi-polar TOF mass  
207 spectrometer. The detectable dynamic mass spectral ion signal is 5-20,000 mV. Before the use of  
208 SPAMS, standard polystyrene latex spheres (0.2-2  $\mu\text{m}$ , Duke Scientific Corp.) and PbCl<sub>2</sub> and  
209 NaNO<sub>3</sub> (0.35  $\mu\text{m}$ , Sigma-Aldrich) solutions were used for the size and mass spectral calibration,  
210 respectively. The hit rate, defined as the ratio of ionized particles to all sampled particles, of the  
211 SPAMS was  $\sim 11\%$  during the cruise observation campaigns.

212       During the R/V *Xuelong* cruise observation campaigns, approximately 930,000 particles with  
213 mass spectral fingerprints and  $D_{va}$  ranging from 0.2 to 2  $\mu\text{m}$  were measured. An adaptive  
214 resonance theory neural network (ART-2a) was used to group the particles into several clusters  
215 based on their mass spectral fingerprints, using parameters of a vigilance factor of 0.85, a learning  
216 rate of 0.05, and a maximum of 20 iterations (Song and Hopke, 1999). The manually obtained  
217 clusters were sea salt (SS, 16.5%), aged sea salt (SS-aged, 8.1%), sea salt with biogenic organic  
218 matter (SS-Bio, 3.1%), internally mixed organics with calcium (OC-Ca, 48.7%), internally mixed  
219 organics with potassium (OC-K, 13.7%), organic-carbon-dominated (OC, 7.0%), and element  
220 carbon (EC, 2.9%) (**Fig. S5 and Table S3**) (Prather et al., 2013; Collins et al., 2014; Su et al.,  
221 2021). All single-particle types had marine origins with typical mass spectral characteristics of Na

222 ( $m/z$  23), Mg ( $m/z$  24), K ( $m/z$  39), Ca ( $m/z$  40), and Cl ( $m/z$  -35 and -37), except for EC (**SI text**  
223 **S2**). There was little difference in individual particle analysis regarding chemical composition,  
224 size, and mixing state of particle clusters obtained from leg I and leg II (**SI Text S3**).

## 225 **3 Results**

### 226 **3.1 Ca<sup>2+</sup> enrichment dominated by environmental factors**

227 We propose that both Na<sup>+</sup> and Ca<sup>2+</sup> in our observations originated from marine sources.  
228 The mass concentration of Na<sup>+</sup> exhibited a strong positive correlation with that of Cl<sup>-</sup> ( $r = 0.99$ ,  
229  $p < 0.001$ ) and Mg<sup>2+</sup> ( $r = 0.99$ ,  $p < 0.001$ ) (**Fig. S6**), indicating that they had a common origin  
230 (i.e., sea spray). However, it is not surprising that the mass concentration of Na<sup>+</sup> showed a  
231 relatively weak correlation with that of Ca<sup>2+</sup> ( $r = 0.51$ ,  $p < 0.001$ ) (**Fig. S6**). This can be  
232 explained by the low water-soluble complexation of Ca<sup>2+</sup> with organic matter and/or insoluble  
233 Ca<sup>2+</sup> in the form of calcareous shell debris, such as CaCO<sub>3</sub>. In addition, the potential impact of  
234 long-range transport of anthropogenic aerosols and dust contributing to Ca<sup>2+</sup> may be limited due  
235 to the predominance of polar air masses during the observation campaigns (**Fig. S2**).

236 The enrichment factor (EF<sub>X</sub>), defined as the mass concentration ratio of a specific species  
237 X to Na<sup>+</sup> in aerosols to that in bulk seawater, is generally used to describe the enrichment extent  
238 of species X in aerosols.

$$239 \text{EF}_X = \frac{([X]/[\text{Na}^+])_{\text{aerosol}}}{([X]/[\text{Na}^+])_{\text{seawater}}}$$

240 An EF<sub>X</sub> > 1 indicates a positive enrichment; otherwise, it indicates depletion. Generally, the  
241 ratio of Ca<sup>2+</sup> to Na<sup>+</sup> in seawater is 0.038 (w/w) (Boreddy and Kawamura, 2015; Su et al., 2022).  
242 During the whole cruise, the hourly average EF<sub>Ca</sub> was  $2.76 \pm 6.27$  (mean  $\pm$  standard deviation (M

243  $\pm$  SD),  $n = 1051$ , ranged from 0.01 to 85, median = 1.18, interquartile range (IQR) = 1.85). Similar  
244 to previous studies (Salter et al., 2016), positive magnesium ( $Mg^{2+}$ ) and potassium ( $K^+$ )  
245 enrichment in SSAs was also observed (**SI text S4**).

246 **Figure 3** presents the enrichment factor of  $Ca^{2+}$  ( $EF_{Ca}$ ) at different ambient temperatures  
247 (separated by a mean value of  $-3.5$  °C), wind speeds (separated by a mean value of  $7$  m  $s^{-1}$ ), and in  
248 the presence/absence of sea ice during the entire observation campaign. The results indicated that  
249 the highest  $EF_{Ca}$  zone ( $M \pm SD = 3.83 \pm 3.43$ , median = 2.66, IQR = 3.37,  $n = 144$ ) occurred at a  
250 lower ambient temperature ( $< -3.5$  °C), lower wind speed ( $< 7$  m  $s^{-1}$ ) and in the presence of sea ice  
251 (**Fig. 3d**). Compared to the contrary conditions (i.e., ambient temperatures  $\geq -3.5$  °C, wind speeds  
252  $\geq 7$  m  $s^{-1}$ , and the absence of sea ice), there was almost calcium depletion ( $EF_{Ca}$ ,  $M \pm SD = 1.01 \pm$   
253  $0.80$ , median = 0.70, IQR = 0.73,  $n = 182$ ) (**Fig. 3c**). Notably, we observed a higher  $EF_{Ca}$  during  
254 the sea ice period than during the period without sea ice ( $3.83 \pm 3.43$  vs.  $2.45 \pm 3.09$  by  $M \pm SD$   
255 and 2.66 vs. 1.18, by median) (**Fig. 3d**), under the conditions of ambient temperatures  $< -3.5$  °C  
256 and wind speeds  $< 7$  m  $s^{-1}$ . In addition, we also observed more frequent  $Ca^{2+}$  enrichment events  
257 during the sea ice period (71.0% in leg I) compared to the period without sea ice (47.7% in leg II)  
258 (**Table S2**). Moreover, the increased  $EF_{Ca}$  varied with decreasing ambient temperature and wind  
259 speed and with increasing sea ice fraction, as shown in **Fig. 4**. Taken together, our results indicate  
260 that the enhanced  $Ca^{2+}$  enrichment in SSAs is sensitive to the lower temperature, lower wind  
261 speeds, and the presence of sea ice.

262 We further analyzed the distribution of  $Ca^{2+}$  enrichment concerning 96-hour back trajectories  
263 with sea ice fraction and chlorophyll-a concentration, as shown in **Fig. 5**. During the observation  
264 campaigns, we identified five areas with continuous enhancement of  $Ca^{2+}$  enrichment, namely,

265 Area 1 and 2 during the leg II, and Area 3,4, and 5 during the leg I. Our results indicated that air  
266 masses traveling over the sea ice and marginal ice zone (> 95%, by trajectory coverage) in Areas 3,  
267 4, and 5, as well as those over the sea ice (28%-33%) and land-based Antarctic ice (57-59%) in  
268 Area 1 and 2, were strongly associated with the increased calcium enrichment (**Table S4**). These  
269 pieces of evidence further support the influence of sea ice on the increased calcium enrichment,  
270 while simultaneously ruling out the influence of long-range transport of anthropogenic aerosol and  
271 dust outside the Antarctic.

272 We observed that a series of high  $EF_{Ca}$  cases in Area 1 were associated with a high  
273 concentration of chlorophyll-a ( $0.99 \pm 1.65 \mu\text{g L}^{-1}$ ). However, it is unlikely that phytoplankton  
274 and/or bacteria are responsible for the enhanced  $EF_{Ca}$  cases due to the weak correlation ( $r = 0.12$ ,  $p$   
275  $< 0.01$ ) between the chlorophyll-a concentration and  $EF_{Ca}$  values (**Fig. S7**). Moreover, although  
276 the ship track of leg II covered large areas with high chlorophyll-a concentrations, the high  $EF_{Ca}$   
277 values were only present at the narrow temporal and spatial scales. Furthermore, results from back  
278 trajectories indicated that air masses did not significantly travel through the region with elevated  
279 chlorophyll-a concentration. Therefore, we suggest that the impact of chlorophyll-a concentration  
280 on  $Ca^{2+}$  enrichment may be limited.

### 281 **3.2 Single-particle characteristics of Ca-containing particles**

282 To elucidate the mixing state of individual calcareous particles, we set a threshold for the ion  
283 count rate of  $m/z$  40  $[Ca]^+$  (ion intensity > 100 mV) to reclassify all single-particle types that were  
284 obtained from the ART-2a algorithm. This means that all reclassified particles contain signals of  
285  $m/z$  40  $[Ca]^+$ . A total of ~ 580, 000 Ca-containing particles were distributed among all particle

286 types, accounting for ~ 62% of the total obtained particles. OC-Ca was the dominant (~ 72%, by  
287 occurrence frequency) particle type among all Ca-containing particles, followed by SS-Ca  
288 (calcium-containing sea salt, ~ 12%) (**Fig. 6h**). Each of the remaining particle types accounted for  
289 negligible fractions (< 7%) in the total of Ca-containing particles, and were classified as “Other”.  
290 Thus, they were not included in the following discussion.

291 OC-Ca was characterized by a prominent ion signature for  $m/z$  at 40  $[\text{Ca}]^+$  in the positive  
292 mass spectrum and organic marker ions of biological origin (e.g., organic nitrogen, phosphate,  
293 carbohydrate, siliceous materials, and organic carbon) in the negative spectrum (**Fig. 6d**).  
294 Specifically, organic nitrogen ( $m/z$  -26  $[\text{CN}]^-$  and -42  $[\text{CNO}]^-$ ) showed the largest number fraction  
295 (NF) at ~88% (**Fig. S5h**), which is likely derived from organic nitrogen species, such as amines  
296 amino groups, and/or cellulose (Czerwiniak et al., 2005; Srivastava et al., 2005; Köllner et al.,  
297 2017; Dall'osto et al., 2019). Higher NFs of phosphate (16%;  $m/z$  -63  $[\text{PO}_2]^-$  and -79  $[\text{PO}_3]^-$ ),  
298 carbohydrates (24%;  $m/z$  -45  $[\text{CHO}_2]^-$ , -59  $[\text{C}_2\text{H}_3\text{O}_2]^-$ , and -73  $[\text{C}_3\text{H}_5\text{O}_2]^-$ ), siliceous materials  
299 (40%;  $m/z$  -60  $[\text{SiO}_2]^-$ ), and organic carbon (37%;  $m/z$  27  $[\text{C}_2\text{H}_3]^-$  and 43  $[\text{C}_2\text{H}_3\text{O}_3]^-$ ) were also  
300 observed in OC-Ca relative to other particle types (**Fig. S5h**). These organic ion signatures likely  
301 correspond to phospholipids, mono- and polysaccharides, and biosilica structures (e.g.,  
302 exoskeletons or frustules), which may be derived from the intact heterotrophic cells, fragments of  
303 cells, and exudates of phytoplankton and/or bacterial (Prather et al., 2013; Guasco et al., 2014;  
304 Zhang et al., 2018). Besides, the strong organic ion intensities may truly reflect the amount of  
305 organic material in OC-Ca, because the particles are sufficiently dry during the ionization process  
306 (i.e., complete positive and negative mass spectra) (Gross et al., 2000). Notably, the possible ion  
307 signals of bromide ( $m/z$  -79 and -81) were observed in OC-Ca, indicating a potential source of

308 blowing snow (Yang et al., 2008; Song et al., 2022).

309 The OC-Ca particles are most likely classified as a distinct SSA population, probably of  
310 marine biogenic origin. Sea salt particles typically exhibit a stronger  $m/z$  23  $[\text{Na}]^+$  than  $m/z$  40  
311  $[\text{Ca}]^+$  due to the higher concentration of  $\text{Na}^+$  vs.  $\text{Ca}^{2+}$  in seawater and also due to the lower  
312 ionization potential of Na vs. Ca (5.14 eV vs. 6.11 eV) (Gross et al., 2000). However, the ratio of  
313  $m/z$  23  $[\text{Na}]^+$  to  $m/z$  40  $[\text{Ca}]^+$  in the OC-Ca particles is reversed, verifying a distinct single particle  
314 type (Gross et al., 2000; Gaston et al., 2011). Similarly, the ion signal of  $m/z$  39  $[\text{K}]^+$  does not  
315 surpass that of  $m/z$  40  $[\text{Ca}]^+$  in OC-Ca, although K is ionized more easily than Ca (4.34 eV vs.  
316 6.11eV) (Gross et al., 2000). Although RH at the sampling outlet was < 40%, the short residence  
317 time of the particles within the drying tube (< 5 s) and vacuum system (< 1 ms) could have been  
318 insufficient for the complete efflorescence of SSAs (Gaston et al., 2011; Sierau et al., 2014).  
319 Hence, the OC-Ca could not be attributed to the chemical fractionation of the efflorescence SSAs  
320 in SPAMS analysis. Additionally, based on the single-particle mass spectrometry technique, some  
321 particle types with similar chemical characteristics to OC-Ca have been observed in both field and  
322 laboratory studies (e.g., atomization of sea ice meltwater collected in the Southern Ocean) (Gaston  
323 et al., 2011; Prather et al., 2013; Collins et al., 2014; Guasco et al., 2014; Dall'osto et al., 2019; Su  
324 et al., 2021). The OC-Ca may be from local emissions because the measurements were almost  
325 entirely influenced by polar air masses (**Fig. S1**). Other possible sources, such as glacial dust  
326 (Tobo et al., 2019), could be excluded because of the lack of crustal mass spectral characteristics  
327 (e.g., -76  $[\text{SiO}_3]^-$ , 27  $[\text{Al}]^+$ , and 48  $[\text{Ti}]^+/64$   $[\text{TiO}]^+$ ) (Pratt et al., 2009; Zawadowicz et al., 2017).  
328 And the mean mass concentration ratio of Ca/Na in the aerosol sample was only 0.10, much lower  
329 than that in the crust (1.78, w/w).



330 In contrast, SS-Ca was classified as a pure inorganic cluster with predominant contributions  
331 of Na-related compounds ( $m/z$  23 [Na]<sup>+</sup>, 46 [Na<sub>2</sub>]<sup>+</sup>, 81/83 [Na<sub>2</sub><sup>35/37</sup>Cl]<sup>+</sup>, and -93/-95 [Na<sup>35/37</sup>Cl<sub>2</sub>]<sup>-</sup>),  
332 Mg ( $m/z$  24), K ( $m/z$  39), and Ca ( $m/z$  40) in the mass spectra (**Fig. 6a**). Organic ion signals such  
333 as organic nitrogen ( $m/z$  -26 [CN]<sup>-</sup> and -42 [CNO]<sup>-</sup>) and phosphate ( $m/z$  -63 [PO<sub>2</sub>]<sup>-</sup> and -79 [PO<sub>3</sub>]<sup>-</sup>)  
334 were rarely detected (~1%, by NF). As described above, these compounds relate to oceanic  
335 biogeochemical processes. In addition, secondary species (e.g., nitrate of  $m/z$  -62 [NO<sub>3</sub>]<sup>-</sup> and  
336 sulfate of  $m/z$  -97 [HSO<sub>4</sub>]<sup>-</sup>) were also not observed, indicating a fresh origin and/or less  
337 atmospheric aging. As a subpopulation of SS, SS-Ca may originate from bubble bursting within  
338 open water and/or blowing snow.

#### 339 **4 Discussion**

340 SS-Ca (calcium-containing sea salt) represents a mixture of NaCl and CaCl<sub>2</sub>. However, the  
341 SS-Ca showed a weak correlation ( $r = 0.21$ ,  $p < 0.05$ , by count and  $r = 0.03$ ,  $p < 0.05$ , by the peak  
342 area of  $m/z$  40 [Ca]<sup>+</sup>) with the mass concentration of Ca<sup>2+</sup> (**Table 1**). In addition, the proportion of  
343 SS-Ca was also small (11.6%, **Fig. 6h**). These results indicate that CaCl<sub>2</sub> is not the major reason  
344 for the Ca<sup>2+</sup> enrichment in SSAs, although CaCl<sub>2</sub> has been proposed as a cause, based on  
345 laboratory atomizing of pure inorganic artificial seawater (Salter et al., 2016). The contribution of  
346 ikaite (CaCO<sub>3</sub>·6H<sub>2</sub>O) could also be excluded due to its low water solubility (Bischoff et al., 1993;  
347 Dieckmann et al., 2008; Dieckmann et al., 2010), although ikaite from sea salt fractionation has  
348 also been proposed to account for the Ca<sup>2+</sup> enrichment in SSAs over the Antarctic coast (Hara et  
349 al., 2012). Moreover, the mass spectral signatures of CaCO<sub>3</sub> (e.g.,  $m/z$  56 [CaO]<sup>+</sup> and -60 [CO<sub>3</sub>]<sup>2-</sup>  
350 (see Sullivan et al. (2009)) were also rare in the SS-Ca particles (**Fig. 6a**).

351 As a major component ( $\sim 72\%$ , by occurrence frequency) of the Ca-containing particles, OC-  
352 Ca is expected to be partially responsible for the calcium enrichment in SSAs. First, the OC-Ca  
353 and mass concentration of  $\text{Ca}^{2+}$  exhibited moderately weak positive correlations ( $r = 0.42$ ,  $p < 0.05$ ,  
354 by count and  $r = 0.49$ ,  $p < 0.05$ , by the peak area of  $m/z$  40  $[\text{Ca}]^+$ ) and moderately strong  
355 correlations under higher  $\text{EF}_{\text{Ca}}$  values ( $\text{EF}_{\text{Ca}} > 10$ ,  $r = 0.63$ ,  $p < 0.05$ , by count and  $r = 0.68$ ,  $p <$   
356  $0.05$ , by the peak area of  $m/z$  40  $[\text{Ca}]^+$ ) (**Table 1**). Also, such correlations were great during leg I ( $r$   
357  $= 0.59$ ,  $p < 0.05$ , by count and  $r = 0.60$ ,  $p < 0.05$ , by the peak area of  $m/z$  40  $[\text{Ca}]^+$ ). Second, the  
358 OC-Ca showed a size distribution with a peak at  $1 \mu\text{m}$  (**Fig. 6i**), which is consistent with the  
359 significant  $\text{Ca}^{2+}$  enrichment that is generally found in submicron SSAs (Cochran et al., 2016;  
360 Salter et al., 2016; Mukherjee et al., 2020).

361 We further show that calcium may strongly mix with organic matter, probably as organically  
362 complexed calcium, in the OC-Ca particles. The calcium correlated well with different kinds of  
363 organic matter (e.g., phosphate,  $r = 0.81$ ,  $p < 0.05$ , by the peak area), but poorly correlated with  
364 chloride ( $r = 0.21$ ,  $p < 0.05$ , by the peak area and  $r = 0.48$ ,  $p < 0.05$ , by mass concentration) (**Fig.**  
365 **S6**). In addition, different kinds of organic matter (e.g., organic nitrogen, organic carbon, etc.) in  
366 the OC-Ca particles also showed enrichment trends below the submicron level, analogously to  
367  $\text{Ca}^{2+}$  enrichment (**Fig. S8**). Particularly,  $\text{EF}_{\text{Ca}}$  and organic nitrogen (with the largest NF in OC-Ca)  
368 were both affected by the environmental factors of ambient temperature, wind speed, and sea ice  
369 fraction, indicating possible organic binding with calcium (**Fig. S9**).

370 To exclude the potential inorganic water-soluble compounds (i.e., chloride ( $m/z$  -35 and -37),  
371 nitrate ( $m/z$  -62), and sulfate ( $m/z$  -97)), we further classified OC-Ca into two subpopulations, OC-  
372 Ca-Organic (23.6%, by proportion) and OC-Ca-Inorganic (48.7%, by proportion) (**Fig. S10**),

373 depending on the presence of inorganic ion signals (i.e., chloride of  $m/z$  -35/-37 [Cl]<sup>-</sup>, nitrate of  
374  $m/z$  -62 [NO<sub>3</sub>]<sup>-</sup>, and sulfate of  $m/z$  -97 [HSO<sub>4</sub>]<sup>-</sup>). Both the OC-Ca types and mass concentrations of  
375 Ca<sup>2+</sup> showed enhanced correlations under high EF<sub>Ca</sub> values (**Table 1**). In particular, OC-Ca-  
376 Organic exhibited stronger correlations than did OC-Ca-Inorganic ( $r = 0.51$  vs.  $r = 0.28$ ,  $p < 0.05$ ,  
377 by count and  $r = 0.51$  vs.  $0.31$ ,  $p < 0.05$ , by the peak area of  $m/z$  40 [Ca]<sup>+</sup>, respectively), which  
378 indicates the importance of OC-Ca-Organic for the enrichment of Ca<sup>2+</sup>. Although we did not  
379 measure the hygroscopicity of the OC-Ca in this study, we infer it to be hygroscopic to some  
380 extent. As reported by Cochran et al. (2017), the mixture of sea salt with organic matter can also  
381 exhibit a certain hygroscopicity (hygroscopicity parameter, 0.50-1.27). Therefore, it is likely that  
382 the organically complexed calcium is slightly water-soluble and is partially responsible for  
383 calcium enrichment, while current studies may neglect it.

384       The possible processes contributing to the calcium enrichment induced by OC-Ca can only  
385 be speculated on (**Fig. 7**). Ca<sup>2+</sup> tends to bind with organic matter of biogenic origin, such as  
386 exopolymer substances (EPSs), and subsequently assemble as marine microgels (Verdugo et al.,  
387 2004; Gaston et al., 2011; Krembs et al., 2011; Orellana et al., 2011; Verdugo, 2012; Orellana et  
388 al., 2021). Large amounts of microgels, driven by sea ice algae, microorganisms, and/or exchanges  
389 of organic matter with the seawater below, stick to the sea ice due to its porous nature.  
390 Furthermore, they are likely to be present in the snow, frost flowers, and brine channels (Krembs  
391 et al., 2002; Gao et al., 2012; Vancoppenolle et al., 2013; Arrigo, 2014; Boetius et al., 2015;  
392 Kirpes et al., 2019). A low wind speed may not only be conducive to the formation of frost flowers  
393 and snow but also produce less sea salt (i.e., small yields of Na<sup>+</sup> relative to Ca<sup>2+</sup>) (Rankin et al.,  
394 2002). Correspondingly, a high wind speed ( $\geq 7 \text{ m s}^{-1}$ ) can yield more sea salt by blowing-snow

395 events and/or wave breaking (Yang et al., 2008; Song et al., 2022), presenting a dilution effect of  
396  $\text{Na}^+$  on  $\text{Ca}^{2+}$ . In this case, the calcium enrichment in SSAs could reasonably be attributed to the  
397 possible gel-like calcium-containing particles released by low-wind-blown sea ice. This inference  
398 is supported by the observation of air masses blown over a large fraction of sea ice/ land-based  
399 Antarctic ice, as well as a moderate negative correlation ( $r = 0.50$ ,  $p < 0.001$ ) between wind speed  
400 and sea ice fraction. In addition, we also observed a higher proportion of OC-Ca at low wind  
401 speeds ( $< 7 \text{ m s}^{-1}$ , 61.5%) than at high wind speeds ( $\geq 7 \text{ m s}^{-1}$ , 38.5%). Coincidentally, Song et al.  
402 (2022) also reported that a low wind-blown sea ice process can drive the biogenic aerosol  
403 response in the high Arctic. In addition, the enhanced presence of film drops was observed at  
404 lower wind speeds ( $< 6 \text{ m s}^{-1}$ ) (Norris et al., 2011), which suggests that the bubble bursts within  
405 the sea ice leads and open water may also be responsible for the release of OC-Ca and its calcium  
406 enrichment involved (Leck and Bigg, 2005b, a; Bigg and Leck, 2008; Leck and Bigg, 2010; Leck  
407 et al., 2013; Kirpes et al., 2019).

408 As expected, the results of the  $\text{Ca}^{2+}$  enrichment in SSAs obtained from ion mass  
409 concentration via IGAC did not fully align with results from SPAMS datasets. We propose two  
410 possible explanations for this discrepancy: (i) It could be attributed to a difference in the size of  
411 particles collected by the two different instruments ( $\sim 10 \mu\text{m}$  for IGAC and  $0.2\text{--}2 \mu\text{m}$  for SPAMS).  
412 In addition, SPAMS cannot measure the Aitken-mode particles (Sierau et al., 2014), and can  
413 measure only the tail of accumulation-mode particles with a relatively low hit rate ( $\sim 11\%$  in this  
414 study). (ii) The types of datasets obtained via IGAC (ion mass concentration) and SPAMS (mass  
415 spectral characteristics) are different. The former method partially reflects the  $\text{Ca}^{2+}$  distribution  
416 based on water-soluble  $\text{Ca}^{2+}$ , while the OC-Ca measured by SPAMS may have low water

417 solubility. The latter method is still challenging to use for quantitative measurements due to  
418 potential inhomogeneities in the transmission efficiencies of the aerodynamic lenses and  
419 desorption/ionization, as well as the matrix effects of individual particles (Gross et al., 2000; Qin  
420 et al., 2006; Pratt and Prather, 2012). Therefore, it may not be straightforward to compare the  
421 particle count and peak area with the absolute mass concentration.

422       Although there is a discrepancy between the two instruments, we believe our results to be  
423 reliable and representative. On the one side, the quantitative results concluded by IGAC confirm  
424 the enrichment of  $\text{Ca}^{2+}$  in SSAs and demonstrate their dependence on and relevance to the  
425 environmental factors. On the other side, the individual particle analysis ranging in size from 0.2  
426 to 2  $\mu\text{m}$  is highly appropriate for revealing the calcium distribution in SSAs, as previous studies  
427 have shown increasing  $\text{Ca}^{2+}$  enrichment in SSAs below 1  $\mu\text{m}$  (Oppo et al., 1999; Hara et al., 2012;  
428 Cochran et al., 2016; Salter et al., 2016; Mukherjee et al., 2020). Our study successfully identifies  
429 a unique calcareous particle type (i.e., OC-Ca) and its specific mixing state. A comprehensive  
430 understanding of the characteristics of OC-Ca to the mechanisms of calcium enrichment is  
431 essential for further recognizing the CCN and IN activation in remote marine areas.

432       Another limitation is that only several environmental factors were considered for calcium  
433 enrichment in this study. Some potential factors, such as surface net solar radiation, snowfall, total  
434 cloud cover, surface pressure, total precipitation, boundary layer height, seawater salinity, etc.,  
435 may also affect the calcium enrichment in SSAs through regulating the yield of sea salt (i.e.,  $\text{Na}^+$   
436 mass concentration) (Song et al., 2022). However, they were not available in this study because of  
437 the lack of measurement during the cruise. Meanwhile, the satellite data with low temporal-spatial  
438 resolution cannot match per hour in each starting condition. We hope that future research will

439 further investigate the enrichment of specific species in SSAs under a wider range of  
440 meteorological or oceanographic conditions.

## 441 **5 Conclusions and atmospheric implications**

442 We investigated the distribution of calcium in SSAs through the R/V *Xuelong* cruise  
443 observation campaigns over the Ross Sea, Antarctica. The most significant  $\text{Ca}^{2+}$  enrichment in  
444 SSAs occurred under relatively lower ambient temperatures ( $< -3.5\text{ }^{\circ}\text{C}$ ) and wind speeds ( $< 7\text{ m s}^{-1}$ )  
445 and with the presence of sea ice. With the help of individual particle mass spectral analysis, we  
446 first propose that a single-particle type of OC-Ca (internally mixed organics with calcium),  
447 probably resulting from the preferential binding of  $\text{Ca}^{2+}$  with organic matter, could partially  
448 account for the calcium enrichment in SSAs. We speculate that OC-Ca is likely produced from the  
449 effects of low wind-blown sea ice on microgels induced by  $\text{Ca}^{2+}$  and/or the bubble bursts in the  
450 open-water and/or sea ice leads. However, the impact of environmental factors and OC-Ca on  
451 calcium enrichment in SSAs still cannot be well predicted by multiple linear regression and  
452 random forest analysis (**SI text S5**), which may be ascribed to other unknown mechanisms and/or  
453 organically complexed calcium with low water solubility. In addition, our conclusions based on  
454 limited spatial, temporal, meteorological, and oceanographic conditions may not be accessible to  
455 other seasons and oceanic basins.

456 We suggest that the environmental behaviors of the possible gel-like calcium-containing  
457 particles (i.e., OC-Ca) should be paid more attention behind the mechanisms of calcium  
458 enrichment. Under the stimulation of specific environmental factors (e.g., pH, temperature,  
459 chemical compounds, pollutants, and UV radiation), their physicochemical properties would be

460 changed (e.g., water-solubility enhanced by the cleavage of polymers) (Orellana and Verdugo,  
461 2003; Orellana et al., 2011). Such particles may be preferred candidates for CCN and/or IN (Willis  
462 et al., 2018; Lawler et al., 2021). To our knowledge, this is the first report of a calcium-dominated  
463 single-particle type OC-Ca in the Antarctic. In the context of global warming and sea ice retreat,  
464 this work provides insight into the chemical composition and distribution of submicron SSAs in  
465 the Antarctic summer atmosphere, which would be helpful for a better understanding of aerosol-  
466 cloud-climate interactions.

#### 467 **Data Availability Statement**

468 The data are available at Zenodo (<https://doi.org/10.5281/zenodo.8279334>). Details can be  
469 accessed by contacting the corresponding author Guohua Zhang ([zhanggh@gig.ac.cn](mailto:zhanggh@gig.ac.cn)) and the first  
470 author Bojiang Su ([subojiang21@mails.ucas.ac.cn](mailto:subojiang21@mails.ucas.ac.cn)).

#### 471 **Declaration of Competing Interest**

472 The authors declare that they have no known competing financial interests or personal  
473 relationships that could have appeared to influence the work reported in this paper.

#### 474 **Author Contributions**

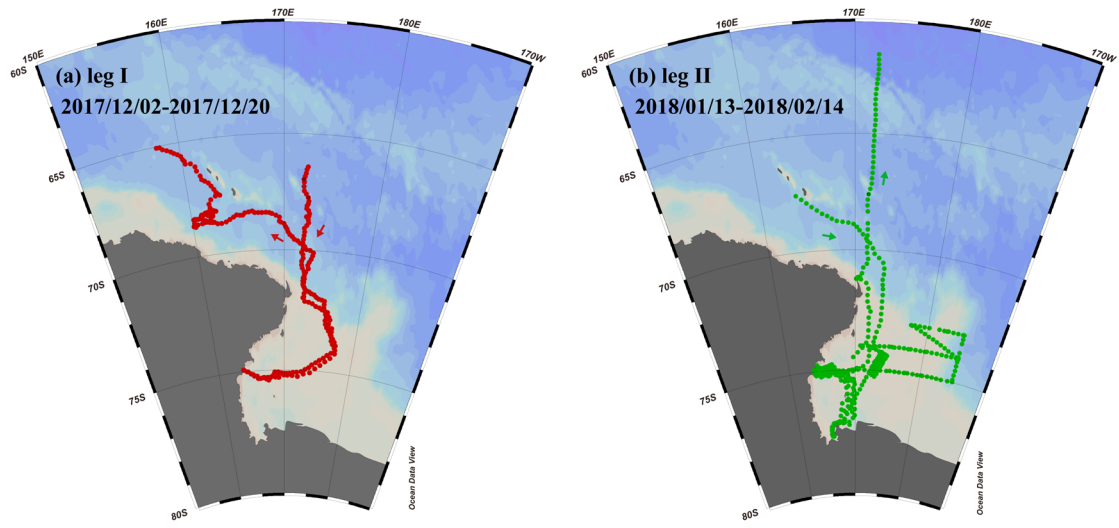
475 The idea for the study was conceived by BJS. BJS analyzed the data, prepared the figures, and  
476 wrote the manuscript under the guidance of GHZ and XYB. LL and JPY contributed to the  
477 observation data. All co-authors contributed to the discussions of the results and refinement of the  
478 manuscript.

479 **Acknowledgment**

480 This work was supported by the National Natural Science Foundation of China (42222705 and  
481 42377097), the Youth Innovation Promotion Association CAS (2021354), the Guangdong Basic  
482 and Applied Basic Research Foundation (2019B151502022), and the Guangdong Foundation for  
483 Program of Science and Technology Research (2020B1212060053). We appreciate the Chinese  
484 Arctic and Antarctic Administration for its support in fieldwork. The authors would like to thank  
485 the editor and reviewers for their valuable time and feedback.



486 **Figure captions**



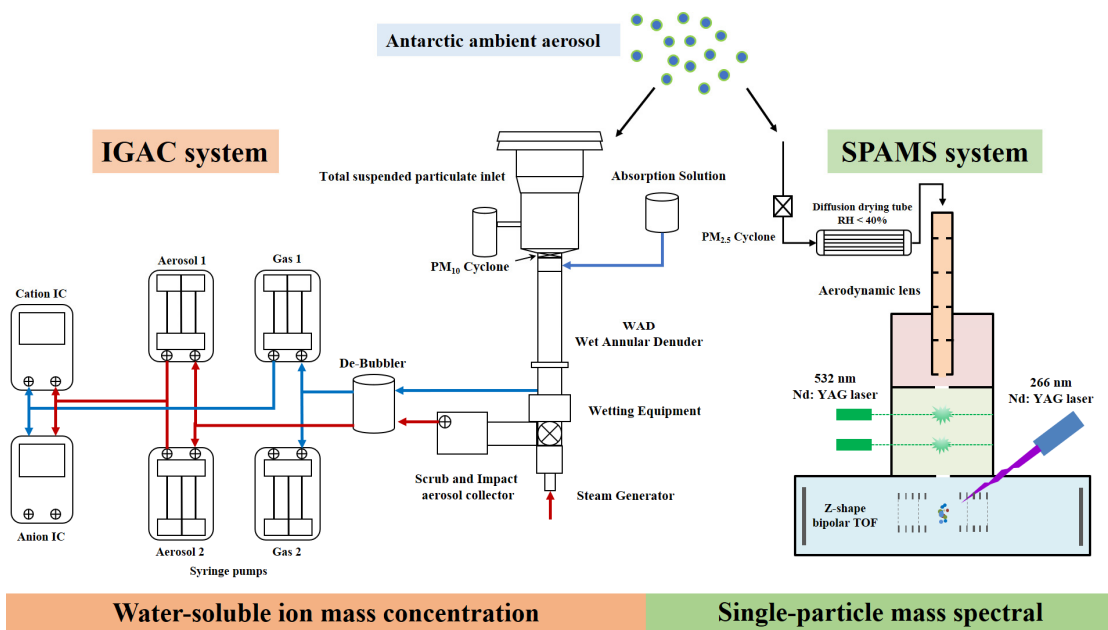
487

488 **Figure 1**

489 Observation campaigns through R/V *Xuelong* in the Ross Sea, Antarctic. (a) Leg I took place from

490 December 2-20, 2017. (b) Leg II was conducted from January 13 to February 14, 2018.

491

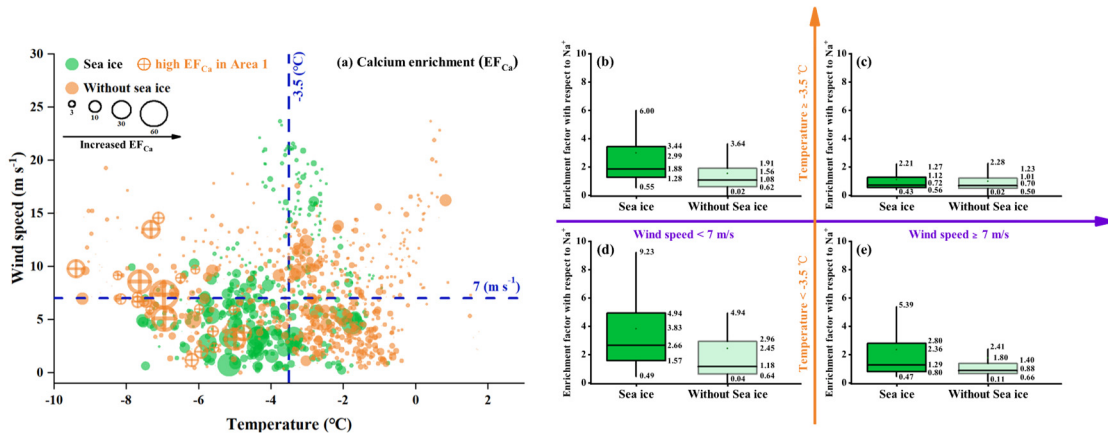


492

493 **Figure 2**

494 A schematic of the aerosol sampling system of IGAC and SPAMS during the research cruise over  
 495 the Ross Sea, Antarctic.

496

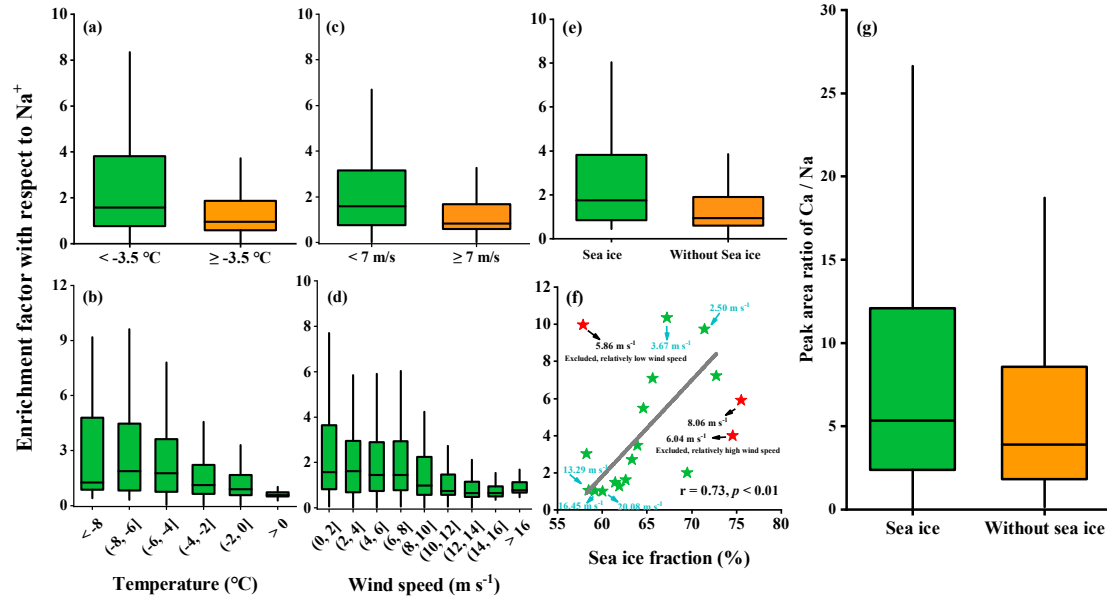


497

498 **Figure 3**

499 (a) Bubble chart of the hourly Ca<sup>2+</sup> enrichment factor (EF<sub>Ca</sub>) with respect to Na<sup>+</sup> with different  
 500 environmental factors (ambient temperature, wind speed, and sea ice fraction). The green and  
 501 orange dots represent the EF<sub>Ca</sub> values for the periods with and without sea ice, respectively. The  
 502 orange marked dots represent a series of high EF<sub>Ca</sub> cases that were correlated with a high  
 503 concentration of chlorophyll-a during leg II of the cruise. (b)-(e) Data support of the bubble chart  
 504 represented by box and whisker plots. In the box and whisker plots, the marked values from top to  
 505 bottom are the 90<sup>th</sup> and 75<sup>th</sup> percentiles, mean, median, and 25<sup>th</sup> and 10<sup>th</sup> percentiles, respectively.

506

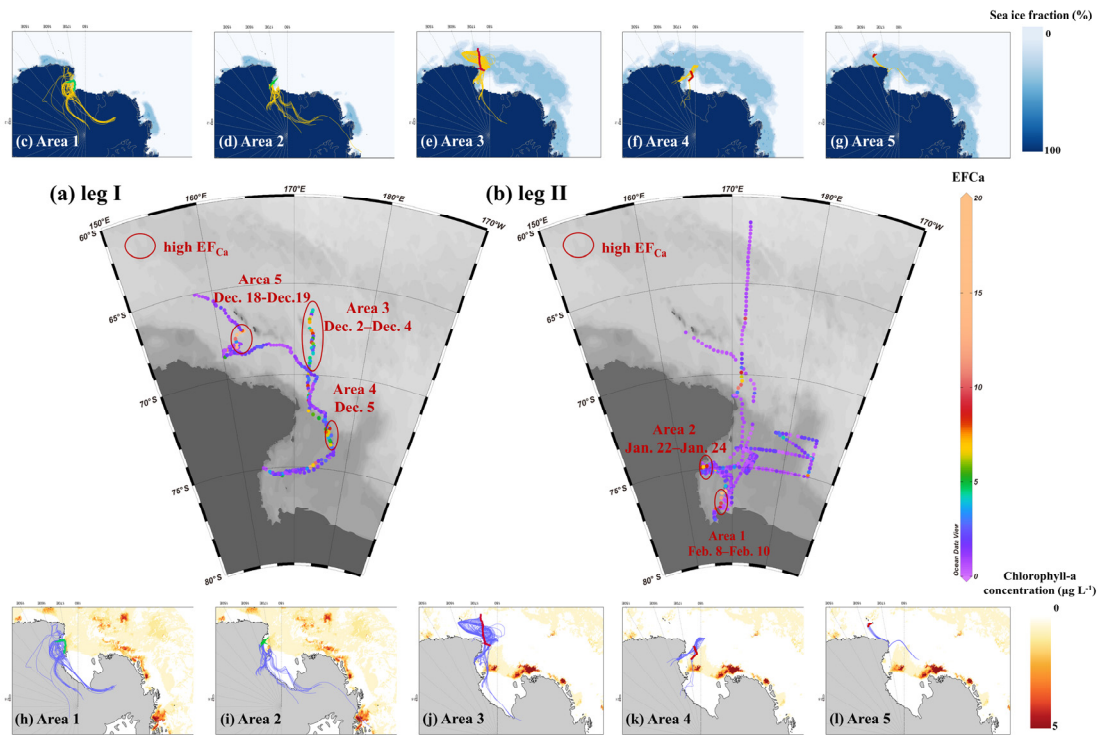


507

508 **Figure 4**

509 Enrichment factors of  $\text{Ca}^{2+}$  with respect to  $\text{Na}^+$  varied as a function of the ambient temperature (a-  
 510 b), wind speed (c-d), and sea ice fraction (e-f) during cruise observation campaigns. (g) A box and  
 511 whisker plot of the single-particle peak area ratio of  $\text{Ca}/\text{Na}$  in OC-Ca for the periods with and  
 512 without sea ice. In the box and whisker plots, the lower, median, and upper lines of the box denote  
 513 the 25<sup>th</sup>, 50<sup>th</sup>, and 75<sup>th</sup> percentiles, respectively. The lower and upper edges denote the 10<sup>th</sup> and  
 514 90<sup>th</sup> percentiles, respectively. The black solid star (f) exhibited an anomalous trend due to its  
 515 nature of relatively high or low wind speed. The first point exhibited a high EF value because of  
 516 its relatively low wind speed ( $5.86\text{ m s}^{-1}$ ). The second and third points exhibited low EF values  
 517 because of their relatively high wind speeds of  $6.04\text{ m s}^{-1}$  and  $8.06\text{ m s}^{-1}$ , respectively. These three  
 518 points have been excluded from the correlation analysis.

519

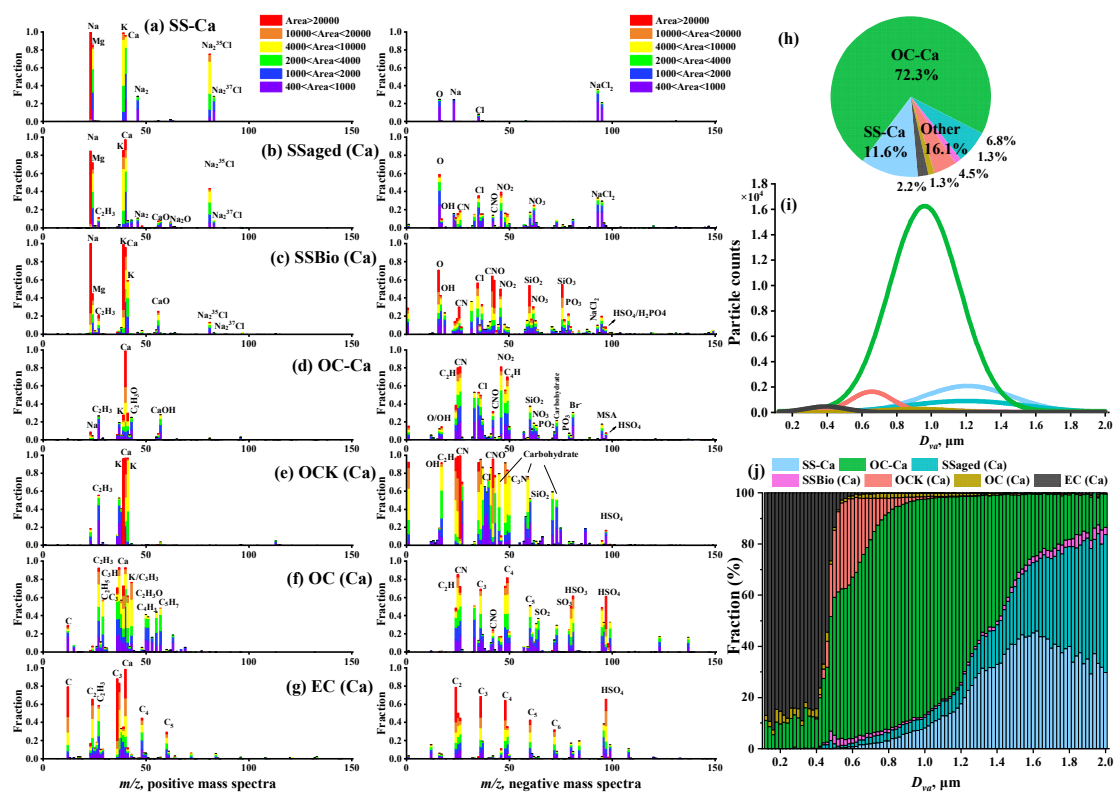


520

521 **Figure 5**

522 Distribution of  $EF_{Ca}$  during (a) leg I and (b) leg II. Five distinct areas with continuous enhanced  
 523  $Ca^{2+}$  enrichment events, along with 96-hour back trajectories (one trajectory per hour in each  
 524 starting condition), sea ice fraction (c-g, yellow traces), and chlorophyll-a concentration (h-l, light-  
 525 blue traces). Lines in red and green referred to ship tracks for corresponding areas during leg I and  
 526 leg II, respectively.

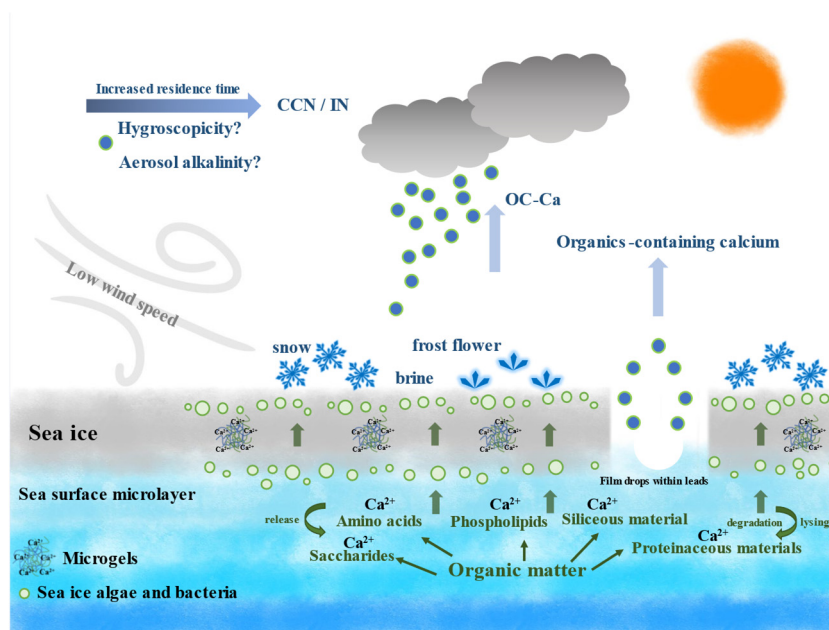
527



529

530 **Figure 6**

531 (a) – (g) Average digitized single-particle mass spectra of seven chemical classes of Ca-containing  
 532 particles. New single-particle types are reclassified with  $m/z$  40 [ $\text{Ca}^{2+}$ ] based on previous ART-2a  
 533 results. (h) Relative proportion and (i) unscaled size-resolved number distributions of single-  
 534 particle types using Gaussian Fitting. (j) Number fractions of single-particle types per size bin  
 535 versus particle size.



536

537 **Figure 7**

538 Schematic of the production of OC-Ca and its possible atmospheric implications beyond calcium  
 539 enrichment.  $Ca^{2+}$  tends to bind with organic matter within sea ice/seawater, and subsequently  
 540 assemble to marine microgels, likely present in the snow, frost flowers, and brine channels. With  
 541 the low wind-blown sea ice process and/or bubble bursting within sea ice leads, these gel-like  
 542 particles (i.e., OC-Ca) may be released to the Antarctic atmosphere, as a potential source of  
 543 CCN/IN. Notably, the dataset via SPAMS cannot directly identify marine microgels. OC-Ca was  
 544 likely associated with marine microgels, as calcium and biological organic material were  
 545 extensively internally mixed. This OC-Ca type has previously been observed in the laboratory  
 546 simulation of Collins et al. (2014).

547

548 **Table captions**

EF <sub>Ca</sub>	Count (Correlation coefficient, r)				Peak area (Correlation coefficient, r, m/z 40 [Ca] <sup>2+</sup> )			
	OC-Ca-Inorganic	OC-Ca-Organic	OC-Ca	SS-Ca	OC-Ca-Inorganic	OC-Ca-Organic	OC-Ca	SS-Ca
0 - 5	0.08	0.31	0.18	0.07	0.18	0.44	0.41	0.04
5 - 10	0.15	0.37	0.27	0.04	0.14	0.36	0.33	0.06
> 10	0.58	0.59	0.63	0.10 <sup>a</sup>	0.53	0.68	0.68	0.10
Leg I	0.45	0.59	0.55	0.02	0.53	0.60	0.60	0.03
Leg II	0.06	0.22	0.14	0.45	0.14	0.39	0.39	0.11
Total	0.28	0.51	0.42	0.21	0.31	0.51	0.49	0.03

a: *p*-value > 0.05  
(Pearson method, two-tailed test)

549

550 **Table 1**

551 Correlation analysis between the OC-Ca (by count and by the peak area of *m/z* 40 [Ca]<sup>+</sup>) and its  
552 two subpopulations OC-Ca-Organic and OC-Ca-Inorganic, SS-Ca (by count and by the peak area  
553 of *m/z* 40 [Ca]<sup>+</sup>), and mass concentration of Ca<sup>2+</sup> in the variation of EF<sub>Ca</sub>, with the *p*-value < 0.05.

554 **References**

- 555 Arrigo, K. R.: Sea ice ecosystems, *Ann Rev Mar Sci*, 6, 439-467, [https://doi.org/10.1146/annurev-](https://doi.org/10.1146/annurev-marine-010213-135103)  
556 [marine-010213-135103](https://doi.org/10.1146/annurev-marine-010213-135103), 2014.
- 557 Bertram, T. H., Cochran, R. E., Grassian, V. H., and Stone, E. A.: Sea spray aerosol chemical  
558 composition: elemental and molecular mimics for laboratory studies of heterogeneous and  
559 multiphase reactions, *Chemical Society Reviews*, 47, 2374-2400,  
560 <https://doi.org/10.1039/c7cs00008a>, 2018.
- 561 Bigg, E. K. and Leck, C.: The composition of fragments of bubbles bursting at the ocean surface,  
562 *Journal of Geophysical Research: Atmospheres*, 113 <https://doi.org/10.1029/2007jd009078>, 2008.
- 563 Bischoff, J. L., Fitzpatrick, J. A., and Rosenbauer, R. J.: The Solubility and Stabilization of Ikaite  
564 (CaCO<sub>3</sub>·6H<sub>2</sub>O) from 0-Degrees-C To 25-Degrees-C - Environmental and Paleoclimatic Implications  
565 for Thionolite Tufa, *J Geol*, 101, 21-33, <https://doi.org/10.1086/648194>, 1993.
- 566 Boetius, A., Anesio, A. M., Deming, J. W., Mikucki, J. A., and Rapp, J. Z.: Microbial ecology of the  
567 cryosphere: sea ice and glacial habitats, *Nat Rev Microbiol*, 13, 677-690,  
568 <https://doi.org/10.1038/nrmicro3522>, 2015.
- 569 Boreddy, S. K. R. and Kawamura, K.: A 12-year observation of water-soluble ions in TSP aerosols  
570 collected at a remote marine location in the western North Pacific: an outflow region of Asian dust,  
571 *Atmos Chem Phys*, 15, 6437-6453, <https://doi.org/10.5194/acp-15-6437-2015>, 2015.
- 572 Brooks, S. D. and Thornton, D. C. O.: Marine Aerosols and Clouds, *Annu Rev Mar Sci*, 10, 289-313,  
573 <https://doi.org/10.1146/annurev-marine-121916-063148>, 2018.
- 574 Carter-Fenk, K. A., Dommer, A. C., Fiamingo, M. E., Kim, J., Amaro, R. E., and Allen, H. C.: Calcium  
575 bridging drives polysaccharide co-adsorption to a proxy sea surface microlayer, *Phys Chem Chem*



576 Phys, 23, 16401-16416, <https://doi.org/10.1039/d1cp01407b>, 2021.

577 Chi, J. W., Li, W. J., Zhang, D. Z., Zhang, J. C., Lin, Y. T., Shen, X. J., Sun, J. Y., Chen, J. M., Zhang, X.  
578 Y., Zhang, Y. M., and Wang, W. X.: Sea salt aerosols as a reactive surface for inorganic and organic  
579 acidic gases in the Arctic troposphere, *Atmos Chem Phys*, 15, 11341-11353,  
580 <https://doi.org/10.5194/acp-15-11341-2015>, 2015.

581 Cochran, R. E., Jayarathne, T., Stone, E. A., and Grassian, V. H.: Selectivity Across the Interface: A  
582 Test of Surface Activity in the Composition of Organic-Enriched Aerosols from Bubble Bursting, *J*  
583 *Phys Chem Lett*, 7, 1692-1696, <https://doi.org/10.1021/acs.jpcllett.6b00489>, 2016.

584 Cochran, R. E., Laskina, O., Trueblood, J. V., Estillore, A. D., Morris, H. S., Jayarathne, T., Sultana, C.  
585 M., Lee, C., Lin, P., Laskin, J., Laskin, A., Dowling, J. A., Qin, Z., Cappa, C. D., Bertram, T. H.,  
586 Tivanski, A. V., Stone, E. A., Prather, K. A., and Grassian, V. H.: Molecular Diversity of Sea Spray  
587 Aerosol Particles: Impact of Ocean Biology on Particle Composition and Hygroscopicity, *Chem.*, 2,  
588 655-667, <https://doi.org/10.1016/j.chempr.2017.03.007>, 2017.

589 Collins, D. B., Zhao, D. F., Ruppel, M. J., Laskina, O., Grandquist, J. R., Modini, R. L., Stokes, M. D.,  
590 Russell, L. M., Bertram, T. H., Grassian, V. H., Deane, G. B., and Prather, K. A.: Direct aerosol  
591 chemical composition measurements to evaluate the physicochemical differences between  
592 controlled sea spray aerosol generation schemes, *Atmos Meas Tech*, 7, 3667-3683,  
593 <https://doi.org/10.5194/amt-7-3667-2014>, 2014.

594 Cravigan, L. T., Mallet, M. D., Vaattovaara, P., Harvey, M. J., Law, C. S., Modini, R. L., Russell, L. M.,  
595 Stelcer, E., Cohen, D. D., Olsen, G., Safi, K., Burrell, T. J., and Ristovski, Z.: Sea spray aerosol  
596 organic enrichment, water uptake and surface tension effects, *Atmos Chem Phys*, 20, 7955-7977,  
597 <https://doi.org/10.5194/acp-20-7955-2020>, 2020.

598 Czerwieńiec, G. A., Russell, S. C., Tobias, H. J., Pitesky, M. E., Fergenson, D. P., Steele, P., Srivastava,  
599 A., Horn, J. M., Frank, M., Gard, E. E., and Lebrilla, C. B.: Stable isotope labeling of entire  
600 *Bacillus atrophaeus* spores and vegetative cells using bioaerosol mass spectrometry, *Anal Chem*,  
601 77, 1081-1087, <https://doi.org/10.1021/ac0488098>, 2005.

602 Dall'Osto, M., Airs, R. L., Beale, R., Cree, C., Fitzsimons, M. F., Beddows, D., Harrison, R. M.,  
603 Ceburnis, D., O'Dowd, C., Rinaldi, M., Paglione, M., Nenes, A., Decesari, S., and Simo, R.:  
604 Simultaneous Detection of Alkylamines in the Surface Ocean and Atmosphere of the Antarctic  
605 Sympagic Environment, *Acs Earth Space Chem*, 3, 854-862,  
606 <https://doi.org/10.1021/acsearthspacechem.9b00028>, 2019.

607 Dieckmann, G., Nehrke, G., Uhlig, C., Göttlicher, J., Gerland, S., Granskog, M., and Thomas, D.: Brief  
608 Communication: Ikaite (CaCO<sub>3</sub>·6H<sub>2</sub>O) discovered in Arctic sea ice, *The Cryosphere*, 4, 227-230,  
609 <https://doi.org/10.5194/tc-4-227-2010>, 2010.

610 Dieckmann, G., Nehrke, G., Papadimitriou, S., Göttlicher, J., Steininger, R., Kennedy, H., Wolf-  
611 Gladrow, D., and Thomas, D.: Calcium carbonate as ikaite crystals in Antarctic sea ice, *Geophys*  
612 *Res Lett*, 35 <https://doi.org/10.1029/2008gl033540>, 2008.

613 Facchini, M. C., Rinaldi, M., Decesari, S., Carbone, C., Finessi, E., Mircea, M., Fuzzi, S., Ceburnis, D.,  
614 Flanagan, R., Nilsson, E. D., de Leeuw, G., Martino, M., Woeltjen, J., and O'Dowd, C. D.: Primary  
615 submicron marine aerosol dominated by insoluble organic colloids and aggregates, *Geophys Res*  
616 *Lett*, 35 <https://doi.org/10.1029/2008gl034210>, 2008.

617 Gao, Q., Leck, C., Rauschenberg, C., and Matrai, P. A.: On the chemical dynamics of extracellular  
618 polysaccharides in the high Arctic surface microlayer, *Ocean Sci*, 8, 401-418,  
619 <https://doi.org/10.5194/os-8-401-2012>, 2012.

620 Gaston, C. J., Furutani, H., Guazzotti, S. A., Coffee, K. R., Bates, T. S., Quinn, P. K., Aluwihare, L. I.,  
621 Mitchell, B. G., and Prather, K. A.: Unique ocean-derived particles serve as a proxy for changes in  
622 ocean chemistry, *Journal of Geophysical Research: Atmospheres*,  
623 116<https://doi.org/10.1029/2010jd015289>, 2011.

624 Gross, D. S., Galli, M. E., Silva, P. J., and Prather, K. A.: Relative sensitivity factors for alkali metal  
625 and ammonium cations in single particle aerosol time-of-flight mass spectra, *Anal Chem*, 72, 416-  
626 422, <https://doi.org/10.1021/ac990434g>, 2000.

627 Guasco, T. L., Cuadra-Rodriguez, L. A., Pedler, B. E., Ault, A. P., Collins, D. B., Zhao, D. F., Kim, M.  
628 J., Ruppel, M. J., Wilson, S. C., Pomeroy, R. S., Grassian, V. H., Azam, F., Bertram, T. H., and  
629 Prather, K. A.: Transition Metal Associations with Primary Biological Particles in Sea Spray  
630 Aerosol Generated in a Wave Channel, *Environ Sci Technol*, 48, 1324-1333,  
631 <https://doi.org/10.1021/es403203d>, 2014.

632 Hara, K., Osada, K., Yabuki, M., and Yamanouchi, T.: Seasonal variation of fractionated sea-salt  
633 particles on the Antarctic coast, *Geophys Res Lett*, 39<https://doi.org/10.1029/2012gl052761>, 2012.

634 Keene, W. C., Maring, H., Maben, J. R., Kieber, D. J., Pszenny, A. A. P., Dahl, E. E., Izaguirre, M. A.,  
635 Davis, A. J., Long, M. S., Zhou, X. L., Smoydzin, L., and Sander, R.: Chemical and physical  
636 characteristics of nascent aerosols produced by bursting bubbles at a model air-sea interface,  
637 *Journal of Geophysical Research: Atmospheres*, 112<https://doi.org/10.1029/2007jd008464>, 2007.

638 Kirpes, R. M., Bonanno, D., May, N. W., Fraund, M., Barget, A. J., Moffet, R. C., Ault, A. P., and Pratt,  
639 K. A.: Wintertime Arctic Sea Spray Aerosol Composition Controlled by Sea Ice Lead  
640 Microbiology, *Acs Central Sci*, 5, 1760-1767, <https://doi.org/10.1021/acscentsci.9b00541>, 2019.

641 Köllner, F., Schneider, J., Willis, M. D., Klimach, T., Helleis, F., Bozem, H., Kunkel, D., Hoor, P.,  
642 Burkart, J., Leaitch, W. R., Aliabadi, A. A., Abbatt, J. P. D., Herber, A. B., and Borrmann, S.:  
643 Particulate trimethylamine in the summertime Canadian high Arctic lower troposphere, *Atmos*  
644 *Chem Phys*, 17, 13747-13766, <https://doi.org/10.5194/acp-17-13747-2017>, 2017.

645 Krembs, C., Eicken, H., and Deming, J. W.: Exopolymer alteration of physical properties of sea ice and  
646 implications for ice habitability and biogeochemistry in a warmer Arctic, *P Natl Acad Sci USA*,  
647 108, 3653-3658, <https://doi.org/10.1073/pnas.1100701108>, 2011.

648 Krembs, C., Eicken, H., Junge, K., and Deming, J. W.: High concentrations of exopolymeric substances  
649 in Arctic winter sea ice: implications for the polar ocean carbon cycle and cryoprotection of  
650 diatoms, *Deep-Sea Res Pt I*, 49, 2163-2181, [https://doi.org/10.1016/S0967-0637\(02\)00122-X](https://doi.org/10.1016/S0967-0637(02)00122-X),  
651 2002.

652 Lawler, M. J., Saltzman, E. S., Karlsson, L., Zieger, P., Salter, M., Baccarini, A., Schmale, J., and Leck,  
653 C.: New Insights Into the Composition and Origins of Ultrafine Aerosol in the Summertime High  
654 Arctic, *Geophys Res Lett*, 48<https://doi.org/10.1029/2021gl094395>, 2021.

655 Leck, C. and Bigg, E. K.: Source and evolution of the marine aerosol - A new perspective, *Geophys*  
656 *Res Lett*, 32<https://doi.org/10.1029/2005gl023651>, 2005a.

657 Leck, C. and Bigg, E. K.: Biogenic particles in the surface microlayer and overlaying atmosphere in the  
658 central Arctic Ocean during summer, *Tellus B*, 57, 305-316, <https://doi.org/10.1111/j.1600-0889.2005.00148.x>, 2005b.

660 Leck, C. and Bigg, E. K.: New Particle Formation of Marine Biological Origin, *Aerosol Sci Tech*, 44,  
661 570-577, <https://doi.org/10.1080/02786826.2010.481222>, 2010.

662 Leck, C. and Svensson, E.: Importance of aerosol composition and mixing state for cloud droplet  
663 activation over the Arctic pack ice in summer, *Atmos Chem Phys*, 15, 2545-2568,

664 <https://doi.org/10.5194/acp-15-2545-2015>, 2015.

665 Leck, C., Gao, Q., Mashayekhy Rad, F., and Nilsson, U.: Size-resolved atmospheric particulate  
666 polysaccharides in the high summer Arctic, *Atmos Chem Phys*, 13, 12573-12588,  
667 <https://doi.org/10.5194/acp-13-12573-2013>, 2013.

668 Li, L., Huang, Z., Dong, J., Li, M., Gao, W., Nian, H., Fu, Z., Zhang, G., Bi, X., Cheng, P., and Zhou,  
669 Z.: Real time bipolar time-of-flight mass spectrometer for analyzing single aerosol particles, *Int J*  
670 *Mass Spectrom*, 303, 118-124, <https://doi.org/10.1016/j.ijms.2011.01.017>, 2011.

671 Liu, Z. M., Lu, X. H., Feng, J. L., Fan, Q. Z., Zhang, Y., and Yang, X.: Influence of Ship Emissions on  
672 Urban Air Quality: A Comprehensive Study Using Highly Time-Resolved Online Measurements  
673 and Numerical Simulation in Shanghai, *Environ Sci Technol*, 51, 202-211,  
674 <https://doi.org/10.1021/acs.est.6b03834>, 2017.

675 Mukherjee, P., Reinfelder, J. R., and Gao, Y.: Enrichment of calcium in sea spray aerosol in the Arctic  
676 summer atmosphere, *Mar Chem*, 227 <https://doi.org/10.1016/j.marchem.2020.103898>, 2020.

677 Murphy, D. M., Anderson, J. R., Quinn, P. K., McInnes, L. M., Brechtel, F. J., Kreidenweis, S. M.,  
678 Middlebrook, A. M., Posfai, M., Thomson, D. S., and Buseck, P. R.: Influence of sea-salt on  
679 aerosol radiative properties in the Southern Ocean marine boundary layer, *Nature*, 392, 62-65,  
680 <https://doi.org/10.1038/32138>, 1998.

681 Norris, S. J., Brooks, I. M., de Leeuw, G., Sirevaag, A., Leck, C., Brooks, B. J., Birch, C. E., and  
682 Tjernstrom, M.: Measurements of bubble size spectra within leads in the Arctic summer pack ice,  
683 *Ocean Sci*, 7, 129-139, <https://doi.org/10.5194/os-7-129-2011>, 2011.

684 Oppo, C., Bellandi, S., Innocenti, N. D., Stortini, A. M., Loglio, G., Schiavuta, E., and Cini, R.:  
685 Surfactant components of marine organic matter as agents for biogeochemical fractionation and  
686 pollutant transport via marine aerosols, *Mar Chem*, 63, 235-253, [https://doi.org/10.1016/S0304-4203\(98\)00065-6](https://doi.org/10.1016/S0304-4203(98)00065-6), 1999.

688 Orellana, M. V. and Verdugo, P.: Ultraviolet radiation blocks the organic carbon exchange between the  
689 dissolved phase and the gel phase in the ocean, *Limnol Oceanogr*, 48, 1618-1623,  
690 <https://doi.org/10.4319/lo.2003.48.4.1618>, 2003.

691 Orellana, M. V., Hansell, D. A., Matrai, P. A., and Leck, C.: Marine Polymer-Gels' Relevance in the  
692 Atmosphere as Aerosols and CCN, *Gels*, <https://doi.org/10.3390/gels7040185>, 2021.

693 Orellana, M. V., Matrai, P. A., Leck, C., Rauschenberg, C. D., Lee, A. M., and Coz, E.: Marine  
694 microgels as a source of cloud condensation nuclei in the high Arctic, *P Natl Acad Sci USA*, 108,  
695 13612-13617, <https://doi.org/10.1073/pnas.1102457108>, 2011.

696 Passig, J., Schade, J., Irsig, R., Li, L., Li, X., Zhou, Z., Adam, T., and Zimmermann, R.: Detection of  
697 ship plumes from residual fuel operation in emission control areas using single-particle mass  
698 spectrometry, *Atmos Meas Tech*, 14, 4171-4185, <https://doi.org/10.5194/amt-14-4171-2021>, 2021.

699 Prather, K. A., Bertram, T. H., Grassian, V. H., Deane, G. B., Stokes, M. D., DeMott, P. J., Aluwihare, L.  
700 I., Palenik, B. P., Azam, F., Seinfeld, J. H., Moffet, R. C., Molina, M. J., Cappa, C. D., Geiger, F.  
701 M., Roberts, G. C., Russell, L. M., Ault, A. P., Baltrusaitis, J., Collins, D. B., Corrigan, C. E.,  
702 Cuadra-Rodriguez, L. A., Ebben, C. J., Forestieri, S. D., Guasco, T. L., Hersey, S. P., Kim, M. J.,  
703 Lambert, W. F., Modini, R. L., Mui, W., Pedler, B. E., Ruppel, M. J., Ryder, O. S., Schoepp, N. G.,  
704 Sullivan, R. C., and Zhao, D. F.: Bringing the ocean into the laboratory to probe the chemical  
705 complexity of sea spray aerosol, *P Natl Acad Sci USA*, 110, 7550-7555,  
706 <https://doi.org/10.1073/pnas.1300262110>, 2013.

707 Pratt, K. A. and Prather, K. A.: Mass spectrometry of atmospheric aerosolsuRecent developments and

708 applications. Part II: On-line mass spectrometry techniques, *Mass Spectrom Rev*, 31, 17-48,  
709 <https://doi.org/10.1002/mas.20330>, 2012.

710 Pratt, K. A., DeMott, P. J., French, J. R., Wang, Z., Westphal, D. L., Heymsfield, A. J., Twohy, C. H.,  
711 Prenni, A. J., and Prather, K. A.: In situ detection of biological particles in cloud ice-crystals, *Nat*  
712 *Geosci*, 2, 397-400, <https://doi.org/10.1038/Ngeo521>, 2009.

713 Qin, X. Y., Bhawe, P. V., and Prather, K. A.: Comparison of two methods for obtaining quantitative  
714 mass concentrations from aerosol time-of-flight mass spectrometry measurements, *Anal Chem*, 78,  
715 6169-6178, <https://doi.org/10.1021/ac060395q>, 2006.

716 Quinn, P. K., Collins, D. B., Grassian, V. H., Prather, K. A., and Bates, T. S.: Chemistry and Related  
717 Properties of Freshly Emitted Sea Spray Aerosol, *Chem Rev*, 115, 4383-4399,  
718 <https://doi.org/10.1021/cr500713g>, 2015.

719 Rankin, A. M., Wolff, E. W., and Martin, S.: Frost flowers: Implications for tropospheric chemistry and  
720 ice core interpretation, *Journal of Geophysical Research: Atmospheres*, 107, AAC 4-1-AAC 4-15,  
721 <https://doi.org/10.1029/2002jd002492>, 2002.

722 Russell, L. M., Hawkins, L. N., Frossard, A. A., Quinn, P. K., and Bates, T. S.: Carbohydrate-like  
723 composition of submicron atmospheric particles and their production from ocean bubble bursting,  
724 *P Natl Acad Sci USA*, 107, 6652-6657, <https://doi.org/10.1073/pnas.0908905107>, 2010.

725 Salter, M. E., Hamacher-Barth, E., Leck, C., Werner, J., Johnson, C. M., Riipinen, I., Nilsson, E. D.,  
726 and Zieger, P.: Calcium enrichment in sea spray aerosol particles, *Geophys Res Lett*, 43, 8277-  
727 8285, <https://doi.org/10.1002/2016gl070275>, 2016.

728 Schill, S. R., Collins, D. B., Lee, C., Morris, H. S., Novak, G. A., Prather, K. A., Quinn, P. K., Sultana,  
729 C. M., Tivanski, A. V., Zimmermann, K., Cappa, C. D., and Bertram, T. H.: The Impact of Aerosol  
730 Particle Mixing State on the Hygroscopicity of Sea Spray Aerosol, *Acs Central Sci*, 1, 132-141,  
731 <https://doi.org/10.1021/acscentsci.5b00174>, 2015.

732 Sierau, B., Chang, R. Y. W., Leck, C., Paatero, J., and Lohmann, U.: Single-particle characterization of  
733 the high-Arctic summertime aerosol, *Atmos Chem Phys*, 14, 7409-7430,  
734 <https://doi.org/10.5194/acp-14-7409-2014>, 2014.

735 Sievering, H.: Aerosol non-sea-salt sulfate in the remote marine boundary layer under clear-sky and  
736 normal cloudiness conditions: Ocean-derived biogenic alkalinity enhances sea-salt sulfate  
737 production by ozone oxidation, *Journal of Geophysical Research: Atmospheres*,  
738 109 <https://doi.org/10.1029/2003jd004315>, 2004.

739 Song, C., Becagli, S., Beddows, D. C. S., Brean, J., Browse, J., Dai, Q., Dall'Osto, M., Ferracci, V.,  
740 Harrison, R. M., Harris, N., Li, W., Jones, A. E., Kirchgäßner, A., Kramawijaya, A. G., Kurganskiy,  
741 A., Lupi, A., Mazzola, M., Severi, M., Traversi, R., and Shi, Z.: Understanding Sources and  
742 Drivers of Size-Resolved Aerosol in the High Arctic Islands of Svalbard Using a Receptor Model  
743 Coupled with Machine Learning, *Environ Sci Technol*, 56, 11189-11198,  
744 <https://doi.org/10.1021/acs.est.1c07796>, 2022.

745 Song, X. and Hopke, P. K.: Classification of single particles analyzed by ATOFMS using an artificial  
746 neural network, *ART-2A, Anal Chem*, 71, 860-865, <https://doi.org/10.1021/ac9809682>, 1999.

747 Srivastava, A., Pitesky, M. E., Steele, P. T., Tobias, H. J., Fergenson, D. P., Horn, J. M., Russell, S. C.,  
748 Czerwieniec, G. A., Lebrilla, C. S., Gard, E. E., and Frank, M.: Comprehensive assignment of  
749 mass spectral signatures from individual *Bacillus atrophaeus* spores in matrix-free laser  
750 desorption/ionization bioaerosol mass spectrometry, *Anal Chem*, 77, 3315-3323,  
751 <https://doi.org/10.1021/ac048298p>, 2005.

752 Su, B., Wang, T., Zhang, G., Liang, Y., Lv, C., Hu, Y., Li, L., Zhou, Z., Wang, X., and Bi, X.: A review  
753 of atmospheric aging of sea spray aerosols: Potential factors affecting chloride depletion, *Atmos*  
754 *Environ*, 290 <https://doi.org/10.1016/j.atmosenv.2022.119365>, 2022.

755 Su, B. J., Zhuo, Z. M., Fu, Y. Z., Sun, W., Chen, Y., Du, X. B., Yang, Y. X., Wu, S., Xie, Q. H., Huang,  
756 F. G., Chen, D. H., Li, L., Zhang, G. H., Bi, X. H., and Zhou, Z.: Individual particle investigation  
757 on the chloride depletion of inland transported sea spray aerosols during East Asian summer  
758 monsoon, *Sci Total Environ*, 765 <https://doi.org/10.1016/j.scitotenv.2020.144290>, 2021.

759 Sullivan, R. C., Moore, M. J. K., Petters, M. D., Kreidenweis, S. M., Roberts, G. C., and Prather, K. A.:  
760 Timescale for hygroscopic conversion of calcite mineral particles through heterogeneous reaction  
761 with nitric acid, *Phys Chem Chem Phys*, 11, 7826-7837, <https://doi.org/10.1039/b904217b>, 2009.

762 Tobo, Y., Adachi, K., DeMott, P. J., Hill, T. C. J., Hamilton, D. S., Mahowald, N. M., Nagatsuka, N.,  
763 Ohata, S., Uetake, J., Kondo, Y., and Koike, M.: Glacially sourced dust as a potentially significant  
764 source of ice nucleating particles, *Nat Geosci*, 12, 253-258, <https://doi.org/10.1038/s41561-019-0314-x>, 2019.

766 Vancoppenolle, M., Meiners, K. M., Michel, C., Bopp, L., Brabant, F., Carnat, G., Delille, B., Lannuzel,  
767 D., Madec, G., Moreau, S., Tison, J.-L., and van der Merwe, P.: Role of sea ice in global  
768 biogeochemical cycles: emerging views and challenges, *Quaternary Science Reviews*, 79, 207-230,  
769 <https://doi.org/10.1016/j.quascirev.2013.04.011>, 2013.

770 Verdugo, P.: Marine microgels, *Annual Review of Marine Science*, 4, 375-400,  
771 <https://doi.org/10.1146/annurev-marine-120709-142759>, 2012.

772 Verdugo, P., Alldredge, A. L., Azam, F., Kirchman, D. L., Passow, U., and Santschi, P. H.: The oceanic  
773 gel phase: a bridge in the DOM-POM continuum, *Mar Chem*, 92, 67-85,  
774 <https://doi.org/10.1016/j.marchem.2004.06.017>, 2004.

775 Wang, Y. Q.: MeteoInfo: GIS software for meteorological data visualization and analysis, *Meteorol.*  
776 *Appl.*, 21, 360-368, <https://doi.org/10.1002/met.1345>, 2014.

777 Wang, Y. Q., Zhang, X. Y., and Draxler, R. R.: TrajStat: GIS-based software that uses various trajectory  
778 statistical analysis methods to identify potential sources from long-term air pollution measurement  
779 data, *Environ Modell Softw*, 24, 938-939, <https://doi.org/10.1016/j.envsoft.2009.01.004>, 2009.

780 Willis, M. D., Leaitch, W. R., and Abbatt, J. P. D.: Processes Controlling the Composition and  
781 Abundance of Arctic Aerosol, *Rev Geophys*, 56, 621-671, <https://doi.org/10.1029/2018rg000602>,  
782 2018.

783 Wilson, T. W., Ladino, L. A., Alpert, P. A., Breckels, M. N., Brooks, I. M., Browse, J., Burrows, S. M.,  
784 Carslaw, K. S., Huffman, J. A., Judd, C., Kilhau, W. P., Mason, R. H., McFiggans, G., Miller, L.  
785 A., Najera, J. J., Polishchuk, E., Rae, S., Schiller, C. L., Si, M., Temprado, J. V., Whale, T. F.,  
786 Wong, J. P., Wurl, O., Yakobi-Hancock, J. D., Abbatt, J. P., Aller, J. Y., Bertram, A. K., Knopf, D.  
787 A., and Murray, B. J.: A marine biogenic source of atmospheric ice-nucleating particles, *Nature*,  
788 525, 234-238, <https://doi.org/10.1038/nature14986>, 2015.

789 Yan, J., Jung, J., Lin, Q., Zhang, M., Xu, S., and Zhao, S.: Effect of sea ice retreat on marine aerosol  
790 emissions in the Southern Ocean, Antarctica, *Sci Total Environ*, 745, 140773,  
791 <https://doi.org/10.1016/j.scitotenv.2020.140773>, 2020a.

792 Yan, J., Jung, J., Zhang, M., Xu, S., Lin, Q., Zhao, S., and Chen, L.: Significant Underestimation of  
793 Gaseous Methanesulfonic Acid (MSA) over Southern Ocean, *Environ Sci Technol*, 53, 13064-  
794 13070, <https://doi.org/10.1021/acs.est.9b05362>, 2019.

795 Yan, J., Jung, J., Zhang, M., Bianchi, F., Tham, Y., Xu, S., Lin, Q., Zhao, S., Li, L., and Chen, L.:

796 Uptake selectivity of methanesulfonic acid (MSA) on fine particles over polynya regions of the  
797 Ross Sea, Antarctica, *Atmos Chem Phys*, 20, 3259-3271, [https://doi.org/10.5194/acp-20-3259-](https://doi.org/10.5194/acp-20-3259-2020)  
798 [2020](https://doi.org/10.5194/acp-20-3259-2020), 2020b.

799 Yang, X., Pyle, J. A., and Cox, R. A.: Sea salt aerosol production and bromine release: Role of snow on  
800 sea ice, *Geophys Res Lett*, 35<https://doi.org/10.1029/2008gl034536>, 2008.

801 Young, L.-H., Li, C.-H., Lin, M.-Y., Hwang, B.-F., Hsu, H.-T., Chen, Y.-C., Jung, C.-R., Chen, K.-C.,  
802 Cheng, D.-H., Wang, V.-S., Chiang, H.-C., and Tsai, P.-J.: Field performance of a semi-continuous  
803 monitor for ambient PM<sub>2.5</sub> water-soluble inorganic ions and gases at a suburban site, *Atmos*  
804 *Environ*, 144, 376-388, <https://doi.org/10.1016/j.atmosenv.2016.08.062>, 2016.

805 Zawadowicz, M. A., Froyd, K. D., Murphy, D. M., and Cziczo, D. J.: Improved identification of  
806 primary biological aerosol particles using single-particle mass spectrometry, *Atmos Chem Phys*, 17,  
807 7193-7212, <https://doi.org/10.5194/acp-17-7193-2017>, 2017.

808 Zhang, T., Fiamingo, M., and Allen, H. C.: Trace Metal Enrichment Driven by Phosphate Functional  
809 Group Binding Selectivity, *Journal of Geophysical Research: Oceans*, 123, 5286-5297,  
810 <https://doi.org/10.1029/2018jc013926>, 2018.

811